IEEE Access
Multidisciplinary | Rapid Review | Open Access Journal

Received November 23, 2020, accepted November 30, 2020, date of publication December 3, 2020,
date of current version December 15, 2020.

Digital Object Identifier 10.1109/ACCESS.2020.3042184

Beam Avoidance for Human Safety in Radiative Wireless Power Transfer

LORENZ GINTING, HYUN SIK YOON, DONG IN KIM, (Fellow, IEEE), AND KAE WON CHOI, (Senior Member, IEEE)

Department of Electrical and Computer Engineering, College of Information and Communication Engineering, Sungkyunkwan University, Suwon 16419, South Korea

Corresponding author: Kae Won Choi (kaewonchoi@skku.edu)

This work was supported in part by the Ministry of Science and ICT (MSIT), South Korea, through the ICT Creative Consilience Program, supervised by the Institute for Information and communications Technology Planning and Evaluation (IITP), under Grant IITP-2020-0-01821, and in part by the National Research Foundation of Korea (NRF) grant funded by the Korean Government (MSIP) under Grant 2014R1A5A1011478.

ABSTRACT Prior studies show that exposure to radio-frequency electromagnetic field (RF-EMF) waves can increase the chance of developing health-related problems. Being exposed to even a small amount of RF-EMF wave emitted from a wireless power transfer (WPT) system for a long time may raise the risk of long-term health effects. Due to this potential human safety issue that may arise from the WPT system, in the future, people may be hesitant to use the RF-based WPT system to charge their electrical devices. To overcome such an issue, we provide an analytical study of a WPT system comprising a single power beacon and multiple target receivers with human bodies in close proximity. We employ a phased antenna array as the transmit and receive antennas to increase the energy transfer efficiency, and model the WPT system as a quadratically constrained quadratic optimization program (QCQP). In this work, we propose two adaptive beam-steering algorithms that maximize the received power on the target receivers while limiting the energy beam to the area where human bodies are detected. In the first proposed algorithm, we apply the semidefinite relaxation (SDR) method to approximate the QCQP solution by relaxing the rank-one constraint. The second proposed algorithm is an optimized adaptive beam-steering method developed by constructing the corresponding dual form of the QCQP problem and solving it through the hierarchical-iterative approach, in which we combine the eigenvalue decomposition and the projected subgradient method to obtain the optimal antenna array weight. Based on the analytical results, both proposed algorithms successfully generate the optimal antenna array weight that steers the main beam toward the target receivers while maintaining the RF-EMF radiation exposure toward the human body below the safety limit. Extensive simulation results are provided for verifying the validness of the proposed algorithms and comparing the performance of these two algorithms. Through testbed implementation, we have shown that the experimental results exhibit good agreement with the simulation results and confirmed the validity of the the proposed algorithm.

INDEX TERMS Beam avoidance, electromagnetic wave exposure, phased antenna array, safe wireless power transfer (WPT).

I. INTRODUCTION

Over a decade, various wireless power transfer (WPT) techniques have been studied to develop a more convenient and efficient charging system for IoT devices. Among all the existing techniques, WPT via radio-frequency electromagnetic field (RF-EMF) radiation has attracted considerable interest recently since the distance between the transmitter and receiver is not limited to a few centimeters. Contrary to the existing off-the-shelf wireless charger that mostly adopts the inductive coupling technique, the RF-based WPT enables the RF waves to travel over a longer distance; thus, the receivers are not restricted to be placed in close proximity to the transmitter.

Despite the advantage of a greater energy transfer range offered by the RF-based WPT, the fact that RF wave power

The associate editor coordinating the review of this manuscript and approving it for publication was Debdeep Sarkar.

dissipates over distance becomes the major challenge to obtain a high power transfer efficiency. In order to address this problem, [1]–[3] use multiple antennas in their WPT system to increase the received power. However, the power transfer efficiency is far from satisfactory since the energy beam spreads all over the WPT area. Therefore, the authors of [4]–[8] adopt the energy beamforming technique to the WPT system for tackling this problem. With the energy beamforming technique, the magnitude and phase of each antenna element can be controlled digitally to generate a constructive beam toward the target receiver location, which yields concentrated energy on the receiver side. Moreover, this approach has been proven to be applied not only to WPT schemes, but also to simultaneous wireless information and power transfer (SWIPT) as in [9] and [10], where the transmitter can send both power and information to the receiver, and wireless powered communication network (WPCN) systems as in [11] and [12], in which the receiver can exploit the received power for communication purposes.

Suppose that the transmitter sends a high amount of power to the receiver. In that case, the energy beamforming technique can become a double-edged sword as the human safety risk may arise due to the overexposure to the RF-EMF radiation when the human body is located near the receiver. To prove the effect of RF-EMF radiation on a human body, the authors of [13] have conducted the experiments using mice. The results of their experiments show that RF-EMF radiation over a long period of time induces cell and tissue degeneration. Another work [14] has also analyzed the problems that possibly arise due to the interaction of RF-EMF radiation with biological systems. Their intensive study shows that not only human health can be affected, but also flora and fauna health can be. The authors also study that RF-EMF radiation can cause several health issues, e.g., headache, eye irritation, fatigue, depression, Alzheimer's disorder, and even cancer. The symptoms may not occur immediately, but they take time to appear as chronic health problems. The work [15] has highlighted the risk of excessive exposure of RF-EMF in the downlink of the 5G communications system, where smaller service cell is deployed. In the 5G network, the base stations equipped with a massive number of antennas are distributed throughout the city, resulting in highly concentrated beams that possibly penetrate the human body. Therefore, the authors encourage the development of a safe downlink cellular system in the 5G technology. Unfortunately, although various WPT techniques have been proposed in recent works, most of them fail to acknowledge the safety issue of the RF WPT.

To circumvent the RF-EMF radiation overexposure issues, the international commission on non-ionizing radiation protection (ICNIRP) issues the guidelines to restrict human body exposure to the RF-EMF radiation. Two metrics which are commonly used in the international guidelines for evaluating human exposure to RF-EMF radiation are the specific absorption rate (SAR) and power density. The SAR is defined as the amount of radiated power absorbed per unit mass of a human body in unit of W/kg, whereas the power density is defined as radiated power per unit area of a human body expressed in unit of W/m^2. In terms of the SAR, the ICNIRP sets 2 W/kg for over 10 g mass as the maximum permissible exposure level, which is equivalent to 5 W/m^2 in terms of the power density. This threshold level can be applied for a transmitter that operates in the frequency range between 100 kHz and 100 GHz [16]. In this paper, we use the power density as a metric to analyze human exposure to RF-EMF radiation. To define a human body area, we assume that each human body is detected by a camera installed at the WPT transmitter. Suppose that the image of a human body formed on the camera image plane has a rectangular-shaped area. This area is further projected on to the far-field (i.e., Fraunhofer) distance away from the optical center of camera using the pinhole camera principle. This projected area on the far-field henceforth refers to a human body area in this paper. Since the human body is assumed to be located in the far-field region, we can define the area of a human body by the set of the elevation and azimuth in the spherical coordinate system.

In this work, we aim at concentrating the RF beams toward the receiver, while limiting the EMF exposure toward the human body. To this end, we formulate the beamforming problem for the WPT system as a quadratically constrained quadratic program (QCQP), which is one of the classes of the convex optimization problem. Frequently, the QCQP problem is addressed by using the semidefinite relaxation (SDR) technique [17]. The SDR has attracted significant interest since it efficiently relaxes a non-convex problem into a convex problem, and the relaxed problem can be solved further in polynomial time by using the available numerical algorithm. However, the solution of the SDR problem does not always result in the optimal QCQP solution due to the relaxation of the rank-1 constraint. To resolve such a problem, the eigenvalue decomposition scheme can be carried out to approximate the QCQP solution.

Despite the great advantage offered by the SDR, the computational complexity of the SDR is quite high, i.e., in the order of $N^{4.5}$ when the number of antenna elements is N [17]. In this work, to alleviate the computational complexity problem, we consider reconstructing the QCQP problem into a simpler problem through the Lagrangian relaxation method [18] and solving it through the two-level hierarchical approach (i.e., inner and outer problems). Lagrangian relaxation simplifies the proposed QCQP problem by adjoining the ''difficult'' inequality constraints to the objective function while the ''easy'' constraint remains as the constraint of the problem. Here, a new variable (i.e., Lagrange multiplier) is introduced to each constraint to construct the additional term formed by a linear combination of the constraints and the corresponding Lagrange multipliers. Afterward, the problem is solved in hierarchical order, in which the eigenvalue decomposition [19], followed by the projected subgradient method [18], are conducted to solve the inner and outer problems, consecutively.

In this paper, we propose two adaptive beam-steering algorithms to address the RF-EMF radiation exposure problem that may arise in the WPT system. To the best of our knowledge, this work is one of a few papers proposing the solution for this safety issue [20]–[22]. The algorithm for a distributed wireless charging system was studied by [20], where the authors use a feedback-based dual ascent method to optimize the transmitted power while satisfying the RF-EMF exposure limit. Instead of using an RF propagation model to estimate the RF-EMF exposure at a specific location, like in their prior work [21], here they use the simulated measurements as feedback to emulate the real-life situation. The distributed charging model is also considered in [22], where the authors approximate the problem with a second-order cone program (SOCP), which can be optimally solved with convex optimization algorithms (e.g., interior-point methods). The authors of [22] consider the jitter of RF-EMF radiation triggered by wireless chargers that is usually overlooked by the prior studies. The other RF radiation-constrained WPT optimization is also presented in [23], where the authors convert the constraints to a multidimensional 0/1 knapsack and a Fermat-Weber problem. Both [22] and [23] conducted a real experiment to test the algorithm performance by using the off-the-shelf devices; Powercast as the wireless charger and sensor node as the receiver. In [24], a beamforming algorithm for multiple-input-single-output (MISO) downlink simultaneous wireless information and power transfer (SWIPT) systems is proposed. In this system model, the author's objective is maximizing the signal-to-interference-plus-noise ratio (SINR) and the harvested power at the receivers, while satisfying the SAR and transmitted power constraints. To do that, the author applies the optimal beamforming and power splitting technique through the semidefinite programming and bisection search.

Among the existing works, none of them particularly considers the phased antenna array as the WPT transmitter and most of the prior works do not consider modeling a human body in the simulation that matches the actual human body area for calculating the power density of RF-EMF radiation exposure on each human body detected in the WPT area. Therefore, in this work, we present the adaptive semidefinite relaxation (SDR) and eigenvalue decomposition/projected subgradient (EVD/PSG) based beam-steering algorithms to solve the RF-EMF radiation overexposure problem that might happen in the WPT system. Our proposed algorithms can decide each antenna element excitation that limits the radiation to a region where a human body is detected while maximizing the received power toward the target receiver by means of the beam focusing technique. To model the human body, we assume a camera is installed in the WPT area to detect the presence of a human body. The human body area is further defined by using the principle of pinhole camera projection that will be rigorously explained in later sections.

The rest of the paper is organized as follows. In Section II, we explain the system model of our work. In Section III, the problem formulation and the proposed solution to avoid the RF-EMF radiation penetrating the human body are provided. In Section IV, we present the numerical simulation results. Section V presents the experimental results, and the paper is concluded in Section VI.

II. SYSTEM MODEL

A. ANTENNA ARRAY CONFIGURATION

The proposed WPT model in this paper comprises a single power beacon and K receivers, each of which is called receiver k (i.e., $k = 1, 2, \ldots, K$). Both power beacon and receiver k are equipped with 2D planar microstrip patch antenna array as their transmit and receive antennas, respectively. The power beacon has N antenna elements, each of them is called antenna n (i.e., $n = 1, 2, \ldots, N$). Every receiver k has M antenna elements and each of them is called antenna m (i.e., $m = 1, 2, \ldots, M$). In our WPT system, N transmit antennas can adaptively focus the RF energy beams towards the receivers, so that they can survive by relying only on the power transmitted by the power beacon.

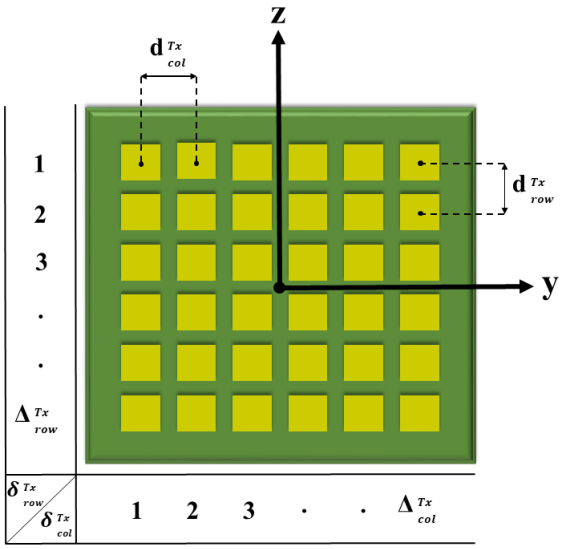

FIGURE 1. Antenna array configuration.

The antenna array configuration for the power beacon and each receiver k is drawn in Fig. 1. As shown in the figure, the antenna array consists of Δ_{col}^{Tx} columns and Δ_{row}^{Tx} rows of antenna elements. The spacing between neighboring antenna elements along y-axis and z-axis are, respectively, d_{col}^{Tx} and d_{row}^{Tx}. The position of each individual antenna element is defined as follows. On the power beacon side, let $\mathbf{s}_n^{Tx} = (s_n^x, s_n^y, s_n^z)^T$ denote the position vector of the phase center of each transmit antenna n in the Cartesian coordinate system,

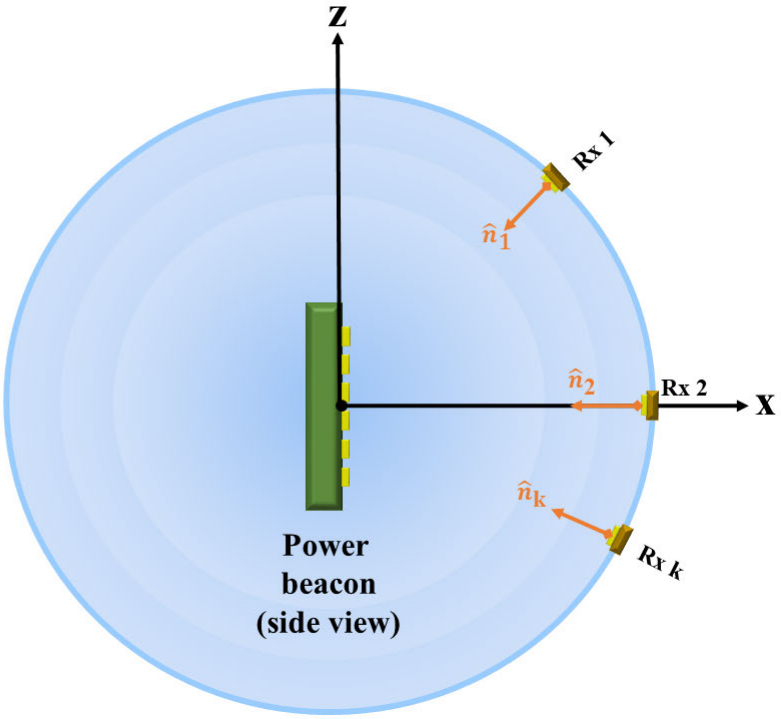

FIGURE 2. Receiver's attitude is restricted to facing towards the power beacon.

and each component of the position vector is defined in terms of its column and row indices (i.e., $(\delta_{col}^{Tx},\ \delta_{row}^{Tx})$) as shown in Fig. 1, such that

$$\begin{aligned} s_n^x &= 0, \\ s_n^y &= \left(\left(\delta_{col}^{Tx} - \frac{1}{2}\right) - \frac{\Delta_{col}^{Tx}}{2}\right) \cdot d_{col}^{Tx}, \\ s_n^z &= \left(\frac{\Delta_{row}^{Tx}}{2} - \left(\delta_{row}^{Tx} - \frac{1}{2}\right)\right) \cdot d_{row}^{Tx}. \end{aligned} \tag{1}$$

On the other hand, each receiver k also has a similar array configuration as the power beacon has, as follows; each receiver k consists of Δ_{col}^{Rx} columns and Δ_{row}^{Rx} rows of antenna elements with the spacing between neighboring antenna array elements denoted by d_{col}^{Rx} and d_{row}^{Rx}.

In our system, we assume that every receiver k is located in the radiative near-field region of the power beacon, and the size of the receiver is much smaller than the power beacon, which leads the power beacon to view the receiver k as a single antenna element, instead of an array of M antenna elements, as depicted in Fig. 2. Consequently, the phase center position of each receiver k can be defined in Spherical coordinate system as $\mathbf{s}_k^{Rx} = (r_k, \theta_k, \phi_k)^T$. This assumption simplifies the calculation of the channel gain from each transmit antenna n towards each receiver k; hence the total received power of each receiver k can be carried out through the summation of the electric field of each transmit antenna n towards one desired direction, $\mathbf{s}_k^{Rx}$.

The positions of the power beacon and receivers in the coordinate system are shown in Fig. 3. In our system model, we assume that the position and attitude of the power beacon are fixed as depicted in the figure; where the power beacon is located on the yz-plane at $x = 0$, with the center of the transmit antenna array at the origin of the coordinate system (i.e., (0, 0, 0)). On the other hand, as stated earlier, every receiver k can be freely located in the radiative near-field region with a minor restriction on the attitude, as illustrated in Fig. 2. As shown in the figure, we assume that a receiver faces towards the power beacon. In other words, the normal vector, denoted $\hat{n}_k$, perpendicular to the surface of receiver k points towards the origin of the coordinate system.

B. POWER WAVE CONCEPT OF ANTENNA CIRCUIT

In this subsection, we explain the concept of the power wave to analyze the transmitted power from the transmit antenna circuit and the received power from the receive antenna circuit. Since both the power beacon and each receiver k consist of multiple antenna ports, we can use the generic multi-port network model to define the scattering parameter of each antenna port, which is usually expressed in terms of the transmitted and received power waves [25]. The transmitted power wave defines the power wave going out from the antenna port, meanwhile received power wave describes the power wave going into the antenna port. We introduce $\mathbf{X}^{Tx} = \left(X_1^{Tx}, X_2^{Tx}, \cdots, X_N^{Tx}\right)^T, \mathbf{X}^{Tx} \in \mathbb{C}^N$, as the column vectors that represent the transmitted power wave at the power beacon.

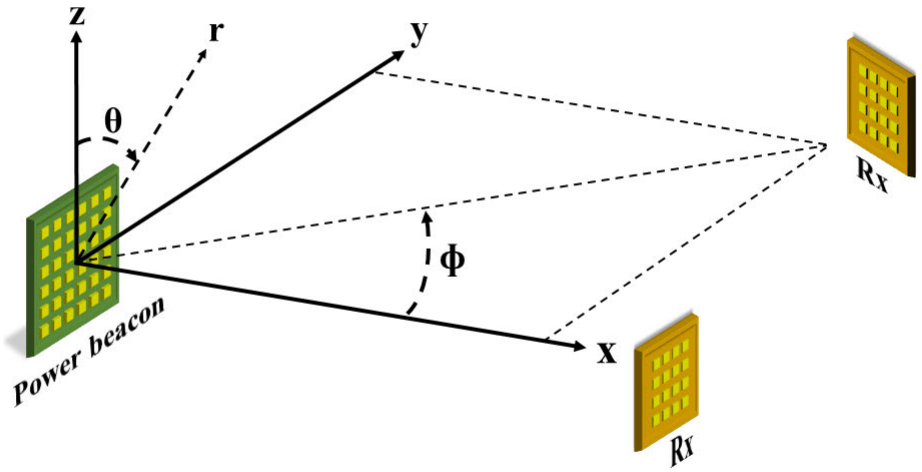

FIGURE 3. WPT system in the Cartesian and spherical coordinate system.

Whereas at receiver k, we introduce the received power wave of receiver k as $\mathbf{X}_k^{Rx} = \left(X_{k,1}^{Rx}, X_{k,2}^{Rx}, \cdots, X_{k,M}^{Rx}\right)^T, \mathbf{X}_k^{Rx} \in \mathbb{C}^M$.

To simplify the overall system model, we assume that no power wave is generated from the antenna ports of receiver k, no power wave is reflected back to the antenna ports of the power beacon, and also no antenna coupling happens between the adjacent antenna elements in the transmit and receive antenna array. Thus, the relation between the transmitted and received power wave at the power beacon and receiver k, respectively, can be simply defined as

$$\mathbf{X}_k^{Rx} = \mathbf{S}_{R_kT}\mathbf{X}^{Tx}, \tag{2}$$

where

$$\mathbf{S}_{R_kT} = \begin{pmatrix} S_{R_{k,1}T_1} & \cdots & S_{R_{k,1}T_N} \\ \vdots & \ddots & \vdots \\ S_{R_{k,M}T_1} & \cdots & S_{R_{k,M}T_N} \end{pmatrix}, \tag{3}$$

$\mathbf{S}_{R_kT} \in \mathbb{C}^{M\times N}$, is a channel gain matrix which describes the relationship between the received power wave at each antenna element m of receiver k and the transmitted power wave from each transmit antenna element n. Since the size of the power beacon is assumed to be much larger than receiver k, every row of $\mathbf{S}_{R_kT}$ has the same value. That is, $S_{R_kT_n} = S_{R_{k,1}T_n} = S_{R_{k,2}T_n} = \cdots = S_{R_{k,M}T_n}$, where $S_{R_kT_n}$ is the channel gain from transmit antenna element n to an antenna element of receiver k. The rigorous calculation of $\mathbf{S}_{R_kT}$ will be explained in later section.

C. RADIATION AND RECEPTION MODEL

In this subsection, we define the RF-EMF radiation wave when transmit antenna port n at the power beacon is excited by power wave X_n^{Tx}. We here assume that both the power beacon and receiver k send the vertically polarized wave, and hence the transferred power loss due to polarization mismatch between the transmit and receive antennas is avoided. In the vertically polarized antenna, the E-plane is an elevation cut, and the electric field is defined in the elevation direction. Let $G_{Tx_n}(\theta_{n,k}, \phi_{n,k})$ denote the gain of the transmit antenna element n towards receiver k, where $\theta_{n,k}$ and $\phi_{n,k}$ denote the elevation and azimuth of receiver k from the transmit antenna element n, respectively. By assuming that each antenna element in the power beacon has the same antenna pattern and $\theta_{n,k} = \theta_k$ and $\phi_{n,k} = \phi_k$ for all n, the gain expression is simplified to $G_{Tx}(\theta_k, \phi_k)$.

Now we can define the E-field at distance $d_{k,n}$ from the phase center of transmit antenna element n towards phase center position of receiver k (i.e., $\mathbf{s}_k^{Rx}$), in terms of transmitted power wave X_n^{Tx} such that

$$E_{\theta,n}^k(\theta_k, \phi_k) = \sqrt{\frac{\eta}{4\pi} \cdot G_{Tx}(\theta_k, \phi_k)} \cdot \frac{1}{d_{k,n}} \times \exp(-j(2\pi/\lambda)d_{k,n}) \cdot X_n^{Tx}, \tag{4}$$

where λ and η denote the wavelength and free-space impedance, respectively. Calculation of $d_{k,n}$ can be carried out in Cartesian coordinate system, such that

$$\begin{aligned} d_{k,n} &= \| \hat{\mathbf{s}}_k^{Rx} - \mathbf{s}_n^{Tx} \|_2 \\ &= \sqrt{(\hat{s}_k^x - s_n^x)^2 + (\hat{s}_k^y - s_n^y)^2 + (\hat{s}_k^z - s_n^z)^2}, \end{aligned} \tag{5}$$

where $\hat{\mathbf{s}}_k^{Rx} = (\hat{s}_k^x, \hat{s}_k^y, \hat{s}_k^z)^T$ is the conversion of $\mathbf{s}_k^{Rx}$ to Cartesian coordinate system such that

$$\begin{aligned} \hat{s}_k^x &= r_k \sin\theta_k \cos\phi_k, \\ \hat{s}_k^y &= r_k \sin\theta_k \sin\phi_k, \\ \hat{s}_k^z &= r_k \cos\theta_k. \end{aligned} \tag{6}$$

In the receiver side, as stated earlier, we assume that every receiver always faces toward the power beacon (i.e., the normal vector $\hat{n}_k$ points toward the coordinate origin), which makes the gain of each receive antenna element m of receiver k constant (i.e., $G_{Rx_{k,m}}(\theta, \phi) = G_{Rx}$). By using the definition

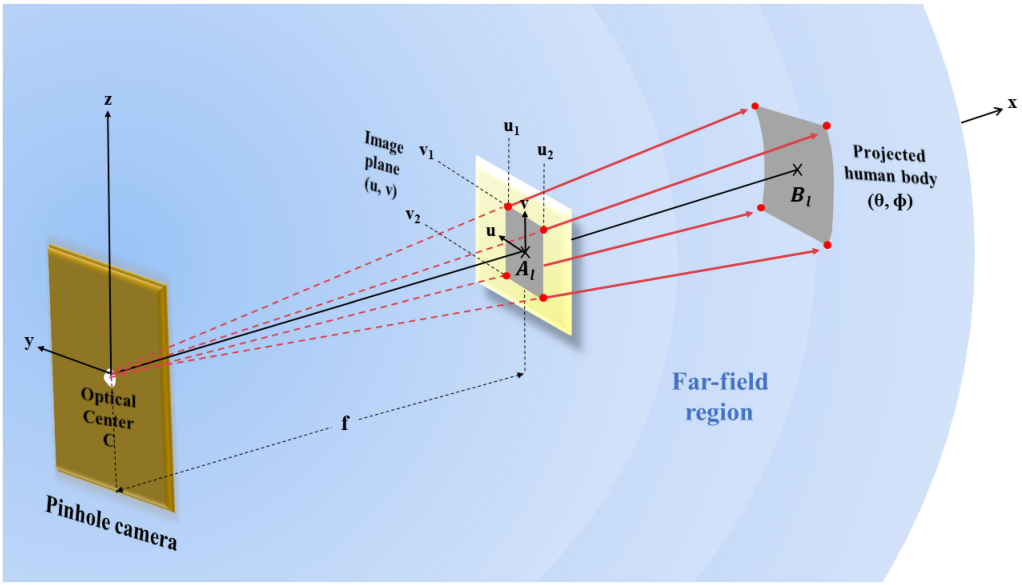

FIGURE 4. Human body model based on the principle of pinhole camera.

of transmit and receive antenna gains, we can define $S_{R_k T_n}$ as the entry of channel gain matrix $\mathbf{S}_{R_k T}$, such that

$$S_{R_k T_n} = \frac{\lambda}{4\pi d_{k,n}} \sqrt{G_{Tx}(\theta_k, \phi_k) G_{Rx}} \times \exp\left(-j(2\pi/\lambda) d_{k,n}\right). \quad (7)$$

D. HUMAN BODY MODEL

In this work, we assume that human body location information is obtained by a camera that is installed at the origin of coordinate system. For mathematical expression, each individual human is modeled by using the principle of pinhole camera as shown in Fig. 4. Suppose there are L human bodies detected around WPT area and each is called human l (i.e., $l = 1, 2, \ldots, L$). The light that passes through the camera hole creates the inverted image of the human body l at distance f behind the optical center C. However, here we assume that the virtual image plane is placed in front of the optical center C at distance f, so that the resulting image is not inverted.

Suppose that the camera projects each human body l onto the virtual image plane. The human body area on the virtual image plane is simply defined as a rectangular shaped area formed by four corner points, which is mathematically defined as $A_l = \{(u, v) \mid u_{l,2} \le u \le u_{l,1},\ v_{l,2} \le v \le v_{l,1}\}$. This rectangular human body area A_l captured by the camera is projected onto the far-field sphere under the assumption that the human body is located in the far-field region of the power beacon. According to Fig. 4, a point in the virtual image plane (u, v) is projected onto a point in the far-field sphere represented by elevation θ and azimuth ϕ as

$$\theta = \arccos\left(v/\sqrt{f^2 + u^2 + v^2}\right), \quad (8)$$

$$\phi = \text{arctan2}(u, f), \quad (9)$$

where f denotes the focal distance and arctan2 (u, f) defines the four-quadrant inverse tangent of u and f. Eventually, the projected human body area on the far-field sphere can be defined as

$$B_l = \{(\theta, \phi) \mid \theta = \arccos\left(v/\sqrt{f^2 + u^2 + v^2}\right), \phi = \text{arctan2}(u, f),\ (u, v) \in A_l\}. \quad (10)$$

III. BEAM FOCUSING AND AVOIDANCE PROBLEM FORMULATION AND SOLUTION

A. WIRELESS POWER TRANSFER TO RECEIVERS

In this subsection, we define the total transmitted and received power by using power wave concept. The transmitted power can be calculated in terms of the transmitted power wave $\mathbf{X}^{Tx}$ as follows

$$P_{Tx} = \frac{1}{2}\|\mathbf{X}^{Tx}\|^2 = \frac{1}{2}\left(\mathbf{X}^{Tx}\right)^H \mathbf{X}^{Tx}, \quad (11)$$

where $\left(\mathbf{X}^{Tx}\right)^H$ denotes the conjugate transpose of $\mathbf{X}^{Tx}$. By using receiver location information, the power beacon concentrates the transmitted power toward the target receiver by means of the beam focusing technique. To calculate the total received power at each receiver k, we use the calculation of the total power wave at receiver k in (2) and the channel gain in (7), such that

$$P_{Rx_k} = \frac{1}{2}\|\mathbf{X}_k^{Rx}\|^2 = \frac{1}{2}\left(\mathbf{X}^{Tx}\right)^H \mathbf{V}_{Rx,k} \mathbf{X}^{Tx}, \quad (12)$$

where $\mathbf{V}_{Rx,k} = \left(\mathbf{S}_{R_k T}\right)^H \mathbf{S}_{R_k T}$, $\mathbf{V}_{Rx,k} \in \mathbb{C}^{N \times N}$.

B. HUMAN BODY EXPOSURE TO RADIATION

In order to calculate the RF radiation exposure on human body l, the equation is given as

$$P_{exp,l} = \int \int_{(\theta,\phi) \in B_l} I_l(\theta, \phi) \sin\theta \, \mathrm{d}\theta \mathrm{d}\phi, \quad (13)$$

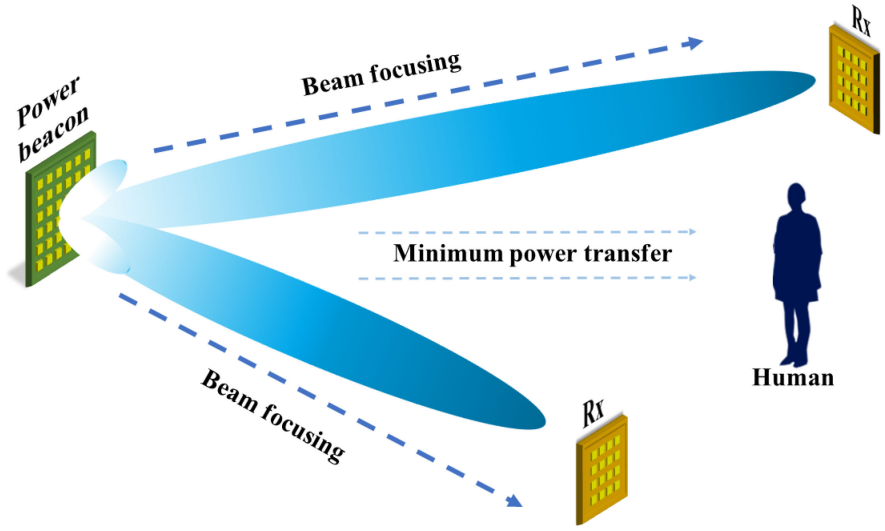

FIGURE 5. Overall proposed WPT system.

where $I_l(\theta, \phi)$ denotes the radiation intensity of the power beacon toward receiver l, which can be derived as

$$I_l(\theta, \phi) = \frac{\left|\sum_{n=1}^{N} \overline{E}_{\theta,n}(\theta, \phi)\right|^2}{2\eta}. \tag{14}$$

As mentioned earlier, we assume that the human body is located in the far-field region of the power beacon. Here, $\overline{E}_{\theta,n}(\theta, \phi)$ is defined as the radiated E-field from transmit antenna element n toward the direction of θ and ϕ at the unit distance. We define $\overline{E}_{\theta,n}(\theta, \phi)$ in terms of the transmitted power wave X_n^{Tx}, such that

$$\overline{E}_{\theta,n}(\theta, \phi) = \sqrt{\frac{\eta}{4\pi} G_{Tx}(\theta, \phi)} \times \exp\left(-j(2\pi/\lambda)\overline{d}_n(\theta, \phi)\right) \cdot X_n^{Tx}, \tag{15}$$

where $\overline{d}_n(\theta, \phi)$ defines the relative distance from transmit antenna n towards the direction of θ and ϕ. The relative distance implies the distance difference between antenna elements, which directly determines the inter-element phase shift. We define $\overline{d}_n(\theta, \phi)$ as

$$\overline{d}_n(\theta, \phi) = s_n^y \sin\theta \sin\phi + s_n^z \cos\theta. \tag{16}$$

From (8), we can rewrite the integral in (13) over the coordinate system (u, v) for the camera image plane by using the determinant of the Jacobian matrix, such that

$$\begin{aligned} &\left|J(u, v)\right| \\ &= \left|\frac{\partial(\theta, \phi)}{\partial(u, v)}\right| = \begin{vmatrix} \frac{\partial\theta}{\partial u} & \frac{\partial\theta}{\partial v} \\ \frac{\partial\phi}{\partial u} & \frac{\partial\phi}{\partial v} \end{vmatrix} \\ &= \begin{vmatrix} \frac{uv(f^2+u^2)^{-\frac{1}{2}}}{f^2+u^2+v^2} & -\frac{(f^2+u^2)^{\frac{1}{2}}}{f^2+u^2+v^2} \\ \frac{f}{f^2+u^2} & 0 \end{vmatrix} = \frac{f(f^2+u^2)^{-\frac{1}{2}}}{f^2+u^2+v^2}. \end{aligned} \tag{17}$$

Based on the calculation above, (13) is converted to

$$P_{exp,l} = \frac{1}{2\eta} \int\int_{(u,v)\in A_l} \left|\sum_{n=1}^{N} \overline{E}_{\theta,n}(\theta, \phi)\right|^2 \times \frac{f}{(f^2+u^2+v^2)^{\frac{3}{2}}} \, du dv. \tag{18}$$

By substituting (15) into (18), the RF radiation exposure to human body l is rewritten as

$$P_{exp,l} = (\mathbf{X}^{Tx})^H \mathbf{V}_{Hu,l} \mathbf{X}^{Tx}, \tag{19}$$

where

$$\mathbf{V}_{Hu,l} = \frac{1}{2\eta} \int\int_{(u,v)\in A_l} \Xi^* \Xi^T \frac{f}{(f^2+u^2+v^2)^{\frac{3}{2}}} \, du dv, \tag{20}$$

$\mathbf{V}_{Hu,l} \in \mathbb{C}^{N\times N}$. Here, we define $\Xi = (\Xi_1, \cdots, \Xi_N)^T$, whose entry is derived as $\Xi_n = \sqrt{\frac{\eta}{4\pi} G_{Tx}(\theta, \phi)} \times \exp(-j(2\pi/\lambda)\overline{d}_n(\theta, \phi))$.

C. OPTIMIZATION PROBLEM FORMULATION

From (11), (12), and (19), we can now formulate an optimization problem for the purpose of maximizing the total received power while maintaining the transmitted power and the RF radiation exposure below a specific limit, as illustrated in Fig. 5, such that

$$\begin{aligned} \underset{\mathbf{X}^{Tx}}{\text{maximize}} \; & \frac{1}{2}\left(\mathbf{X}^{Tx}\right)^H \cdot \sum_{k=1}^{K} \left(\mathbf{V}_{Rx,k}\right) \cdot \mathbf{X}^{Tx}, \\ \text{subject to} \; & \frac{1}{2}\left(\mathbf{X}^{Tx}\right)^H \cdot \mathbf{X}^{Tx} = P_{Tx}^{max} \\ & \left(\mathbf{X}^{Tx}\right)^H \cdot \mathbf{V}_{Hu,l} \cdot \mathbf{X}^{Tx} \le P_{exp}^{max}, \\ & \text{for all} \quad l = 1, \cdots, L, \\ & \frac{1}{2}\left(\mathbf{X}^{Tx}\right)^H \cdot \mathbf{V}_{Rx,k} \cdot \mathbf{X}^{Tx} \ge P_{Rx}^{min}, \\ & \text{for all} \quad k = 1, \cdots, K. \end{aligned} \tag{21}$$

Here, we set $P_{Tx}^{max} \in \mathbb{R}$ and $P_{exp}^{max} \in \mathbb{R}$ as the maximum limit of transmitted power and electromagnetic radiation exposure level for human body l, respectively. In addition, $P_{Rx}^{min} \in \mathbb{R}$ denotes the minimum received power for each receiver. Since the objective function and constraints are written in the quadratic form, the optimization problem above is categorized as the quadratically constrained quadratic problem (QCQP). The optimal solution of this problem is denoted by $\mathbf{X}_{opt}^{Tx}$.

This optimization problem is a non-convex problem since $\mathbf{V}_{Rx,k}$ is a positive semidefinite matrix which makes the objective function and the third constraint non-convex. Hence, this problem cannot be simply solved by using the available convex optimization solvers (i.e., CVX and SeDuMi).

D. SOLUTION ALGORITHM

1) SEMIDEFINITE RELAXATION (SDR)

We can solve (21) by using the semidefinite relaxation technique [17]. To this end, we convert (21) into the following form by using a trace operator Tr.

$$\begin{aligned}
\underset{\mathbf{Z}}{\text{maximize}}\ & \frac{1}{2}\,\text{Tr}\left(\sum_{k=1}^{K}\left(\mathbf{V}_{Rx,k}\right)\cdot\mathbf{Z}\right)\\
\text{subject to}\ & \frac{1}{2}\,\text{Tr}\left(\mathbf{I}\cdot\mathbf{Z}\right)=P_{Tx}^{max}\\
& \text{Tr}\left(\mathbf{V}_{Hu,l}\cdot\mathbf{Z}\right)\le P_{exp}^{max},\quad \text{for all } l=1,\cdots,L\\
& \frac{1}{2}\,\text{Tr}\left(\mathbf{V}_{Rx,k}\cdot\mathbf{Z}\right)\ge P_{Rx}^{min},\ \text{for all } k=1,\cdots,K\\
& \text{rank}\left(\mathbf{Z}\right)=1,\\
& \mathbf{Z}\succeq 0,
\end{aligned}\tag{22}$$

where $\mathbf{Z} = (\mathbf{X}^{Tx})^H \cdot \mathbf{X}^{Tx}$. Here, $\mathbf{Z}$ is a rank-one positive semidefinite (PSD) matrix (i.e., $\text{rank}(\mathbf{Z}) = 1$ and $\mathbf{Z} \succeq 0$). Among the equations in (22), the only non-convex one is the rank constraint (i.e., $\text{rank}(\mathbf{Z}) = 1$). Therefore, to solve the problem effectively, we can relax the above optimization problem to a convex optimization problem by releasing this rank constraint such that

$$\begin{aligned}
\underset{\mathbf{Z}}{\text{maximize}}\ & \frac{1}{2}\,\text{Tr}\left(\sum_{k=1}^{K}\left(\mathbf{V}_{Rx,k}\right)\cdot\mathbf{Z}\right)\\
\text{subject to}\ & \frac{1}{2}\,\text{Tr}\left(\mathbf{I}\cdot\mathbf{Z}\right)=P_{Tx}^{max}\\
& \text{Tr}\left(\mathbf{V}_{Hu,l}\cdot\mathbf{Z}\right)\le P_{exp}^{max},\quad \text{for all } l=1,\cdots,L\\
& \frac{1}{2}\,\text{Tr}\left(\mathbf{V}_{Rx,k}\cdot\mathbf{Z}\right)\ge P_{Rx}^{min},\ \text{for all } k=1,\cdots,K\\
& \mathbf{Z}\succeq 0.
\end{aligned}\tag{23}$$

Since the relaxed optimization problem is convex, we can solve the problem in polynomial time by using the available convex problem algorithm, e.g., interior point method [18].

2) EIGENVALUE DECOMPOSITION/PROJECTED SUBGRADIENT (EVD/PSG)

Other than the semidefinite relaxation, we also propose an algorithm based on the combination of the eigenvalue decomposition and projected subgradient techniques. We reformulate the optimization problem (21) into the relaxed problem through the Lagrange multiplier method, such that

$$\begin{aligned}
\underset{\mathbf{X}^{Tx}}{\text{maximize}}\ & \frac{1}{2}\left(\mathbf{X}^{Tx}\right)^H\cdot\mathbf{A}\cdot\mathbf{X}^{Tx}+\mathbf{B}\\
\text{subject to}\ & \frac{1}{2}\left(\mathbf{X}^{Tx}\right)^H\cdot\mathbf{X}^{Tx}=P_{Tx}^{max},
\end{aligned}\tag{24}$$

where we define $\mathbf{A}$ such that

$$\mathbf{A}=\frac{1}{2}\sum_{k=1}^{K}\mathbf{V}_{Rx,k}-\sum_{l=1}^{L}\lambda_{Hu,l}\cdot\mathbf{V}_{Hu,l}+\frac{1}{2}\sum_{k=1}^{K}\lambda_{Rx,k}\cdot\mathbf{V}_{Rx,k}\tag{25}$$

and $\mathbf{B}$ as

$$\mathbf{B}=\sum_{l=1}^{L}\lambda_{Hu,l}\cdot P_{exp}^{max}-\sum_{k=1}^{K}\lambda_{Rx,k}\cdot P_{Rx}^{min}.\tag{26}$$

Here, $\lambda_{Rx,k} \in \mathbb{R}$ and $\lambda_{Hu,l} \in \mathbb{R}$ are introduced as the dual variables of the problem which are defined as the control coefficients to ensure that the constraints of received power and RF radiation exposure are satisfied.

To solve the relaxed problem, we adopt the hierarchical procedure, in which we break down the optimization problem into the inner and outer problems. In the inner problem, the optimization problem (24) is solved under the condition that the dual variables are fixed. Since $\mathbf{B}$ is a constant, we can remove $\mathbf{B}$ from (24), and cast the problem into the eigenvalue problem, which can be solved through the eigenvalue decomposition such that

$$\mathbf{A}=\mathbf{\Psi}\mathbf{Q}\mathbf{\Psi}^H.\tag{27}$$

Here, $\mathbf{\Psi}$ is an N-by-N matrix, whose nth column represents the eigenvector $\boldsymbol{\psi}_n$ of $\mathbf{A}$, such that $\mathbf{\Psi} = (\boldsymbol{\psi}_1, \boldsymbol{\psi}_2, \cdots, \boldsymbol{\psi}_N)$. Along with $\mathbf{\Psi}$, we define $\mathbf{Q}$ as an N-by-N diagonal matrix, whose entry represents the corresponding eigenvalue (i.e., $\mathbf{Q}_{nn} = q_n$) sorted in a descending order. Since our objective function is maximizing the power, we select the principal eigenvector of $\mathbf{A}$ (i.e., $\boldsymbol{\psi}_1$) to find the optimal $\mathbf{X}^{Tx}$, that is

$$\mathbf{X}^{Tx}(\lambda_{Rx,k},\lambda_{Hu,l})=\sqrt{2P_{Tx}^{max}}\cdot\boldsymbol{\psi}_1,\tag{28}$$

where $\mathbf{X}^{Tx}(\lambda_{Rx,k}, \lambda_{Hu,l})$ is defined as the optimal $\mathbf{X}^{Tx}$ given the dual variables, $\lambda_{Rx,k}$ and $\lambda_{Hu,l}$.

In the outer problem, we find the optimal solution for the dual variables $\lambda_{Rx,k}$ and $\lambda_{Hu,l}$ by using the projected subgradient method. The projected subgradient method updates the dual variables as

$$\lambda_{Hu,l}^{(i+1)}=\left[\lambda_{Hu,l}^{(i)}+\gamma_{Hu,l}\left(P_{exp,l}^{(i)}-P_{exp}^{max}\right)\right]_+,\tag{29}$$

$$\lambda_{Rx,k}^{(i+1)}=\left[\lambda_{Rx,k}^{(i)}+\gamma_{Rx,k}\left(P_{Rx}^{min}-P_{Rx,k}^{(i)}\right)\right]_+,\tag{30}$$

where i denotes the iteration number, $\lambda_{Hu,l}^{(i)}$ and $\lambda_{Rx,k}^{(i)}$ are the dual variables at the ith iteration, and $\gamma_{Rx,k}$ and $\gamma_{Hu,l}$ represent the constant step sizes that are assigned to control the convergence rate of $P_{Rx,k}$ and $P_{exp,l}$, respectively. In (29) and (30), $P_{exp,l}^{(i)}$ and $P_{Rx,k}^{(i)}$ are the exposure level and receive power at the ith iteration such that

$$P_{exp,l}^{(i)} = (\mathbf{X}^{Tx,(i)})^H \cdot \mathbf{V}_{Hu,l} \cdot \mathbf{X}^{Tx,(i)}, \tag{31}$$

$$P_{Rx,k}^{(i)} = \frac{1}{2}(\mathbf{X}^{Tx,(i)})^H \cdot \mathbf{V}_{Rx,k} \cdot \mathbf{X}^{Tx,(i)}, \tag{32}$$

where $\mathbf{X}^{Tx,(i)} = \mathbf{X}^{Tx}(\lambda_{Rx,k}^{(i)}, \lambda_{Hu,l}^{(i)})$. In every iteration, $\lambda_{Rx,k}$, $\lambda_{Hu,l}$, and $\mathbf{X}^{Tx}(\lambda_{Rx,k}, \lambda_{Hu,l})$ are updated through (27)–(32) and continue to be updated until $\lambda_{Rx,k}$ and $\lambda_{Hu,l}$ reach the convergence state.

For this algorithm, the EVD and PSG computation are executed separately, in which the EVD procedure is performed prior to the PSG method. As mentioned earlier, the EVD method works with N-by-N matrix, hence $\mathcal{O}(N^3)$ time suffices to do the computation [26]. On the other hand, the convergence rate of PSG theoretically is $\mathcal{O}(1/\varepsilon^2)$, which implies the complexity depends on the desired accuracy ε, not the number of antenna element N. In the PSG method, we update and check the feasibility of the dual variable $\lambda_{Hu,l}$ and $\lambda_{Rx,k}$ in every iteration without the needs to perform a specific number of iterations (i.e., N). By applying this hierarchical approach, the only complexity that takes into account is only the EVD complexity. Hence, the proposed EVD/PSG algorithm has lower complexity than the SDR method (i.e., $\mathcal{O}(N^{4.5})$).

IV. SIMULATION RESULTS AND ANALYSIS

We have carried out various simulations to assess the proposed analytical model and equations presented in the previous sections. In the simulation, we model the power beacon (Tx) and the receiver (Rx) as phased patch antenna arrays, which work at the operating frequency of 5.8 GHz. Furthermore, the human body is represented by a rectangle with dimension 0.5 m-by-1.7 m (i.e., width-by-height). As explained in the previous section, in the algorithm, we assume that the human body is in far-field region. However, for the simulation, we conduct a more reliable calculation of the RF radiation exposure power on the human body by integrating the Poynting vectors that go over the human body area, hence the human body is not restricted to be placed in the far-field region.

A. SINGLE RECEIVER

In this subsection, we set up the first simulation scenario of a WPT system consisting of one transmitter, one receiver, and a person in a 6 m-by-10 m square area. Here, the transmitter and receiver are modeled as 16-by-16 and 8-by-8 phased antenna arrays, respectively. The simulation layout is depicted in Fig. 6 in which the transmitter is located at (0 m, 0 m) and the receiver is at (7 m, 0 m) in the X-Y plane. Here, we consider the person moves along the X-axis from 3 m to 10 m. In this simulation, we set the $P_{Tx}^{max} = 2$ W,

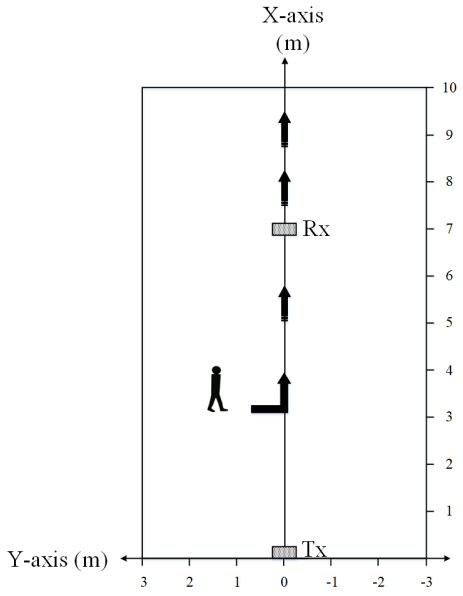

FIGURE 6. Single receiver simulation layout.

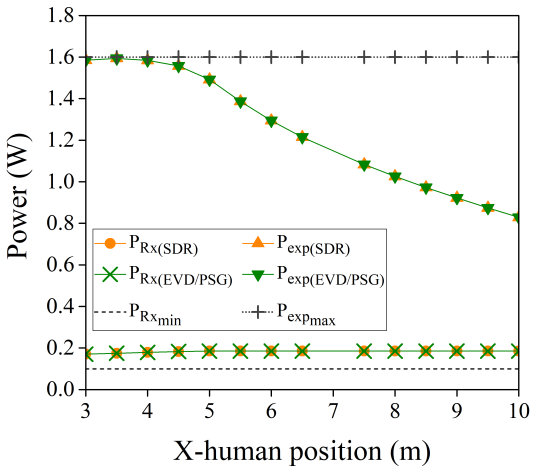

FIGURE 7. Received power and RF radiation exposure power according to human movement along X-axis.

$P_{Rx}^{min} = 0.1$ W, and $P_{exp}^{max} = 1.6$ W. As a result, Fig. 7 shows the received power and exposure power for various positions of the person. From the figure, we can see that the exposure power is kept within the safe exposure level at distance 3 m and decreases as the person moves further away from the transmitter. This phenomenon indicates that the EMF power decreases over distance, thus we can infer that the closer the human body to the power beacon, the greater the amount of EMF power exposed to the human body is. On the other hand, the received power slightly increases but does not notably change that much because we disregard the blockage models to simplify the simulation. As a comparison, we also provide the results obtained from the semidefinite relaxation (SDR) algorithm. We can observe that the SDR results well match the eigenvalue decomposition/projected

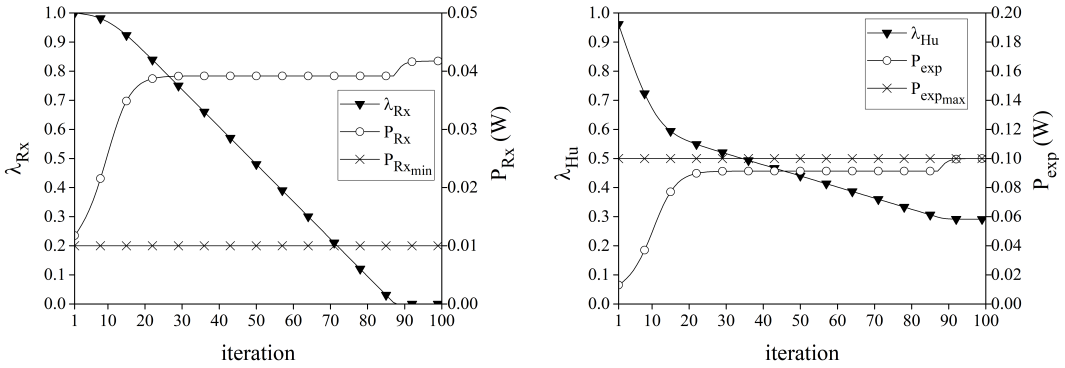

(a) λ_{Rx}, P_{Rx} vs iteration number

(b) λ_{Hu}, P_{exp} vs iteration number

FIGURE 8. Convergence graphs of single receiver case.

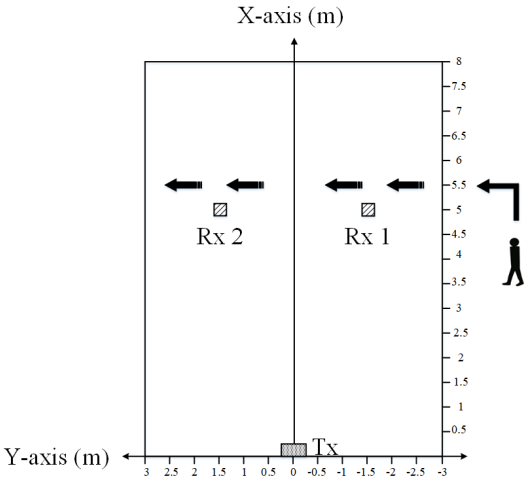

FIGURE 9. Multiple receivers simulation layout.

subgradient (EVD/PSG) results, which indicates that the EVD/PSG algorithm is comparable to the SDR algorithm while having a lower complexity.

For the purpose of observing the convergence process in the EVD/PSG method, we present Fig. 8 to show the received power and exposure power with the corresponding λ_{Rx} and λ_{Hu} as the function of the iteration number. In this figure, we set up the second simulation scenario, in which we use a 16-by-16 phased antenna array as the transmitter and an 8-by-8 antenna array as the receiver. We place the transmitter, receiver, and human body at (0 m, 0 m), (6 m, 0 m), and (7 m, 0 m), respectively, and we use the projected subgradient method with a constant step size (i.e., $\gamma_{Rx} = 0.01$, $\gamma_{Hu} = 0.01$). From the graphs, we can observe that as the dual variables (i.e., λ_{Rx} and λ_{Hu}) are updated by using the projected subgradient method until converge to the optimal dual solution, the primal variables (i.e., P_{Rx} and P_{exp}) concurrently reaches the near-optimal solution.

B. MULTIPLE RECEIVERS

For the case of multiple receivers, the layout is depicted in Fig. 9. Here, we consider the WPT system comprising one transmitter (denoted by Tx), two receivers (denoted by Rx 1 and Rx 2), and a person inside a 6 m-by-8 m square area. In this subsection, we always consider the transmitter to be a 16-by-16 phased antenna array and each receiver as an 8-by-8 phased antenna array. For this simulation, receivers 1 and 2 are located at (5 m, −1.5 m) and (5 m, 1.5 m), respectively, in the X-Y plane. Here, we set $P_{Tx}^{max} = 1$ W, $P_{Rx}^{min} = 0.01$ W, and $P_{exp}^{max} = 0.1$ W. As shown in the figure, the person moves horizontally along the Y-axis from −2.5 m to 2.5 m while the X-axis position is kept at 5.5 m. In this scenario, we expect to observe how human body position affects the energy beam shape and the received power of each receiver. In Fig. 10, various energy beam shapes according to human body position are presented. Here, the beam shape is constructed from the calculation of the Poynting vector that is tangential to the X-Y plane. From the results, we observe that the transmit beam splits toward each receivers and varies its concentration based on human body location. As the person gets closer to a receiver, the energy beam tends to be less concentrated to avoid the RF-EMF overexposure.

To confirm the accuracy of the results, in Fig. 11, we plot the received power and exposure power as the function of the human body position. The notable difference between the received power of Rx 1 and Rx 2 appears when the human stands close to one of the receivers, which is around $Y = -1.5$ m and $Y = 1.5$ m. In other words, when the human stands closer to one receiver, the transmitter suppresses the energy toward that receiver and focuses the energy toward another receiver to avoid the EMF overexposure. Although the transferred power is restrained to the receiver which locates closer to the human body, the received power of that receiver is still well maintained above the minimum received power limit (P_{Rx}^{min}). From the figure, we can also observe that the EVD/PSG results are almost identical to the SDR results. Based on the results, we can conclude that both the proposed algorithms successfully assure the human safe from the RF-EMF radiation overexposure since all the EMF exposure power always stays within the range of the permissible exposure limit.

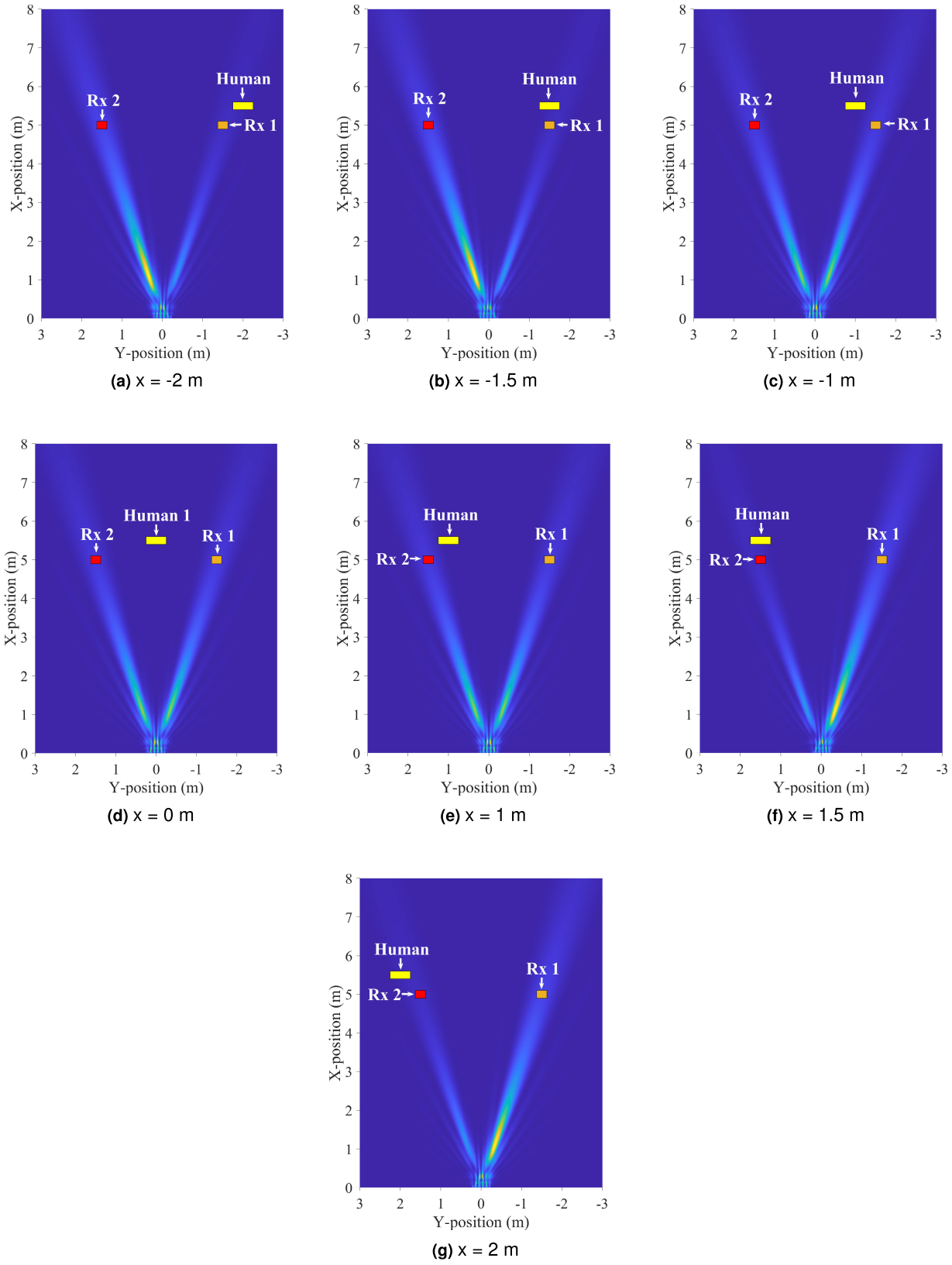

FIGURE 10. Various beam shapes according to human position: two receivers and one person case.

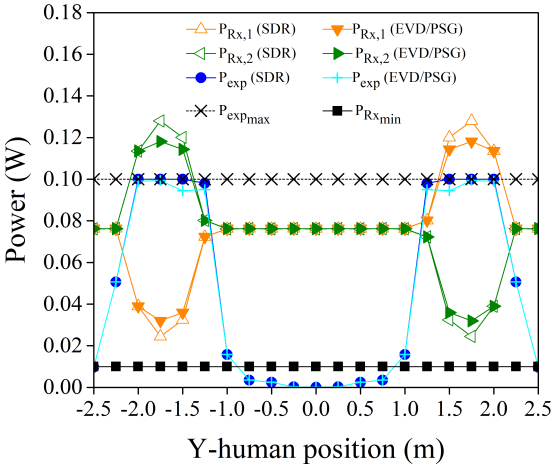

FIGURE 11. Received power and RF radiation exposure power according to human movement along Y-axis.

Fig.12 shows the convergence analysis of the EVD/PSG algorithm for the case of multiple receivers. In this simulation, the first receiver (Rx 1), second receiver (Rx 2), and human body are placed at (5 m, −0.5 m), (5 m, 0.5 m), and (6 m, 0.5 m), respectively. We set the same constant step size as in the single receiver case. Since the person stands closer to Rx 2, our algorithm tends to send more power to Rx 1 than Rx 2. Meanwhile, as the iteration goes, the EMF exposure toward the human body gradually converges and stays below the safety limit. From the figure, we can see that as the dual variables (i.e., $\lambda_{Rx,1}$, $\lambda_{Rx,2}$, and λ_{Hu}) are iteratively updated until they converge after the 90th iteration, the primal variables (i.e., P_{Rx} and P_{exp}) gradually reach the state of the convergence as well. This figure does validate that our optimization problem can be solved through the proposed EVD/PSG algorithm.

In the next scenario, we increase the number of people around the WPT area to check if the EVD/PSG algorithm can handle such a situation. Here, we set $P_{Tx}^{max} = 2$ W, $P_{Rx}^{min} = 0.01$ W, and $P_{exp}^{max} = 0.2$ W. We put the receivers and people in two different positions and generate the corresponding beam shapes, as presented in Fig. 13. The corresponding received and exposure power results are provided in Fig. 14. In Fig. 13(a), the transmitter sends more power to Rx 2 since there is a human stands in front of Rx 1. Therefore, to avoid overexposure, the transmitter focuses the energy toward Rx 2 while maintaining an adequate power supply to Rx 1. Meanwhile, in Fig. 13(b), we can observe that the distance in X-direction from Rx 1 to Human 1 is closer than Rx 2 to Human 2, thus the transmit beam tends to be more concentrated toward Rx 2. From these plots, we can see that the algorithm works well in focusing the power toward the receivers and avoiding the human for the case of two receivers and two people.

In the last scenario, we assume four receivers and two people in the WPT area and set up the $P_{Tx}^{max} = 2$ W, $P_{Rx}^{min} = 0.01$ W, and $P_{exp}^{max} = 0.2$ W. Various beam patterns are generated and shown in Fig. 15. Along with the beam shape plots, we also provide the received power of each receiver and the exposure power of each human for every case in Fig. 16. Here, we can observe that the results yield good agreement between the beam shapes and the received and exposure power plots for every case. Based on the results, we confirm that the proposed algorithm performs properly when the number of receivers is increased. We can conclude that our proposed algorithm can adjust the optimal antenna weights based on human position, which results in the right amount of power delivered toward each receiver without violating the RF-EMF restriction.

V. EXPERIMENTAL RESULTS AND ANALYSIS

A. TESTBED MODEL

As shown in Fig. 17, we have built a testbed and conducted the experiments to validate the proposed EVD/PSG algorithm. The testbed consists of a 4-by-8 linearly-polarized phased antenna array as the transmit antenna and a horn antenna as the receiver, both operate on the 5.8 GHz frequency band. Each transmit antenna element is associated with a digital phase shifter with 5.625° resolution for adjusting the excitation phase. In order to verify whether the power wave ($\mathbf{X}^{Tx}$) obtained from EVD/PSG algorithm is feasible to be used in the real testbed environment, we transfer the phase angle of $\mathbf{X}^{Tx}$, which is generated by our MATLAB simulation, to the LabVIEW software, which works as the main controller in this experiment. The LabVIEW software assigns the excitation phase and delivers it to the phase shifter of each transmit antenna element. Afterward, the weights are converted to the RF energy signal and wirelessly transmitted toward the horn antenna. Next, the received RF power on the horn antenna is measured by the digital power meter; thus, the beam shape can be generated.

The coordinate system of the experimental setup follows the coordinate system of our system model depicted in Fig. 3, in which the transmit antenna array lies in yz-plane and radiates the RF energy toward the x-axis direction. To draw the beam pattern, we placed the transmit antenna on the turntable, which rotates at a constant velocity in a clockwise direction from the $\phi = -45°$ to 45°, and mounted the horn antenna on the antenna mast whose height can be adjusted to cover the elevation angle from $\theta = 65°$ to 115°. Both the turntable and the antenna mast are electronically controlled from the LabVIEW software.

B. EXPERIMENTAL RESULT

In this subsection, The EVD/PSG algorithm is validated by the comparison with the experimental data. To compare the experimental and simulation results, we performed the MATLAB simulation beforehand, obtained the phase angle of the power wave, and implemented it in the testbed by using a LabVIEW program. The results we obtained from the simulation and experiment are shown in Fig. 18. Here, we consider the WPT system comprising one transmitter,

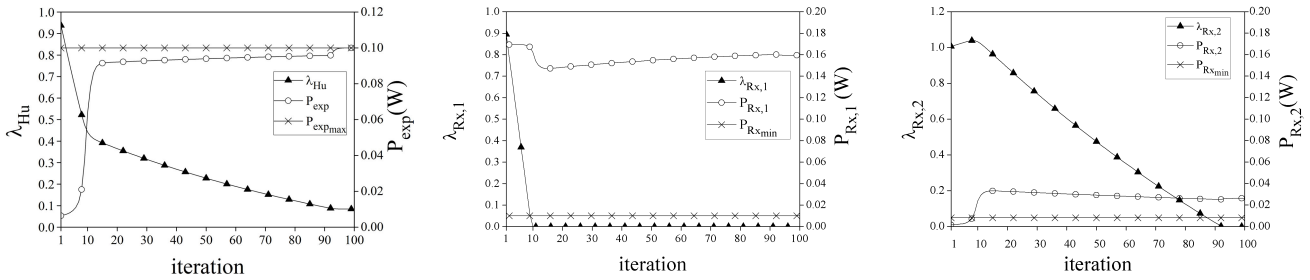

(a) λ_{Hu}, P_{exp} vs iteration number (b) $\lambda_{Rx,1}$, $P_{Rx,1}$ vs iteration number (c) $\lambda_{Rx,2}$, $P_{Rx,2}$ vs iteration number

FIGURE 12. Convergence graphs of two receivers and one human case.

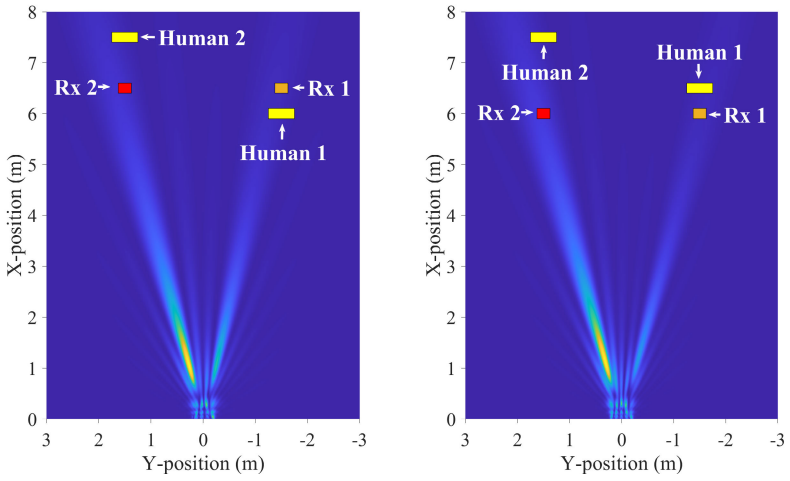

(a) Case a (b) Case b

FIGURE 13. Various beam shapes according to human position: two receivers and two people case.

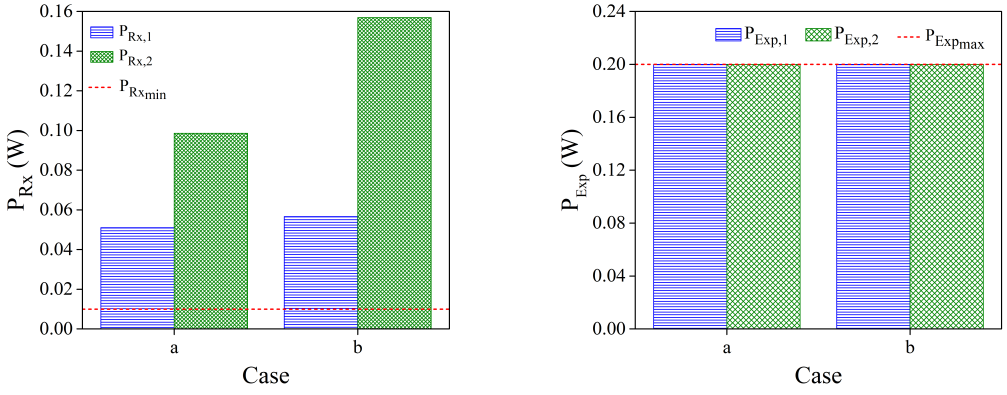

(a) Received power (b) Exposure power

FIGURE 14. Received power and RF radiation exposure power of two receivers and two people case.

two receivers, and a person, and we set the $P_{Tx}^{max} = 4$ W, $P_{Rx}^{min} = 0.01$ W, and $P_{exp}^{max} = 0.1$ W. Throughout the simulations, the first receiver (Rx 1) and second receiver (Rx 2) are placed at (3 m, −1.5m) and (3 m, 1.5 m), respectively, but the position of the person varies to three different positions: at (3.5 m, 0 m), (3.5 m, −1.5 m), and (3.5 m, 1.5 m), consecutively. From the figure, a fairly good agreement between the simulation and experiment is shown. Two beams are formed, which shows that the power beacon focuses the energy towards both receivers. Moreover, we can clearly observe that

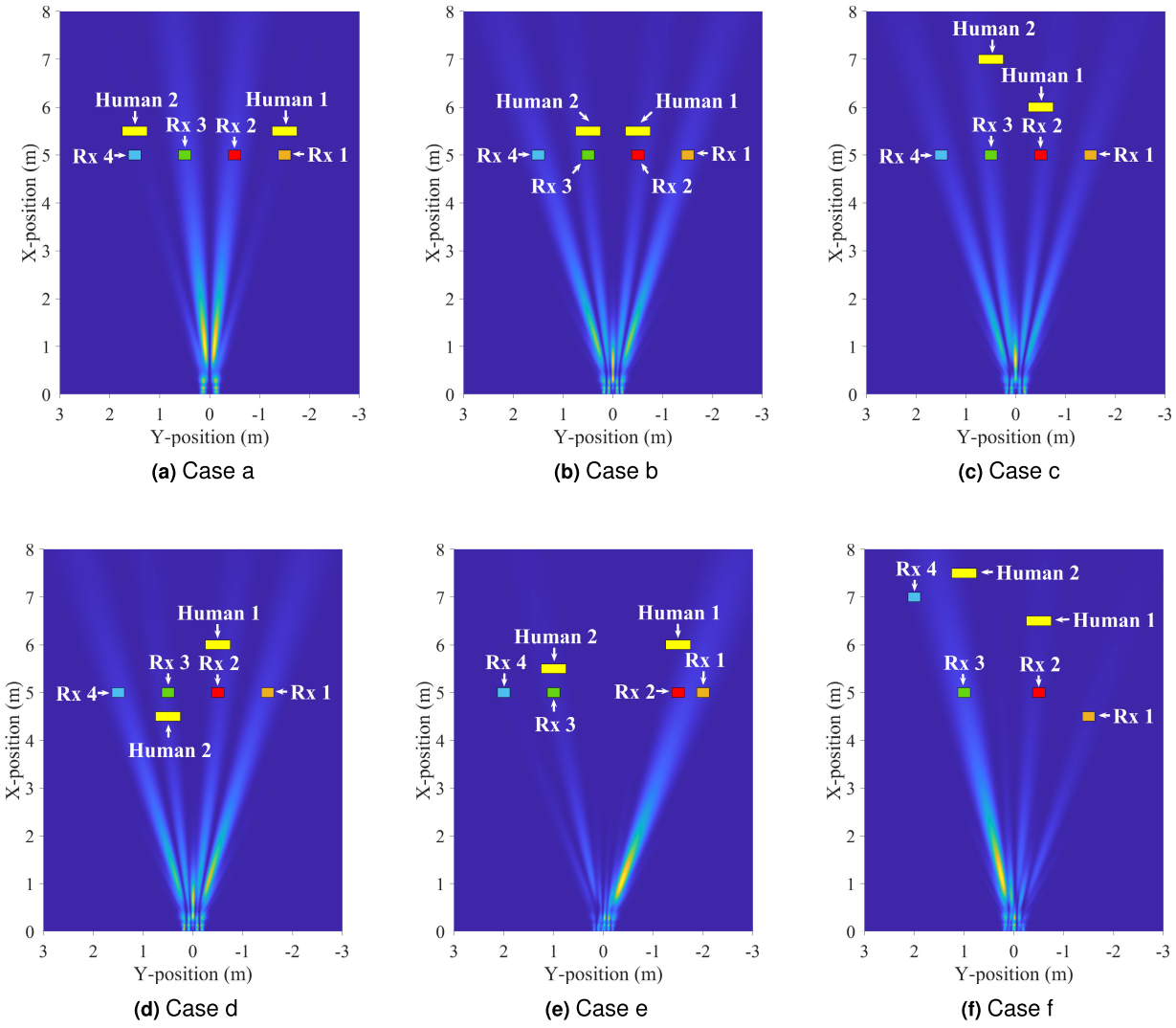

FIGURE 15. Various beam shapes according to human position: four receivers and two people case.

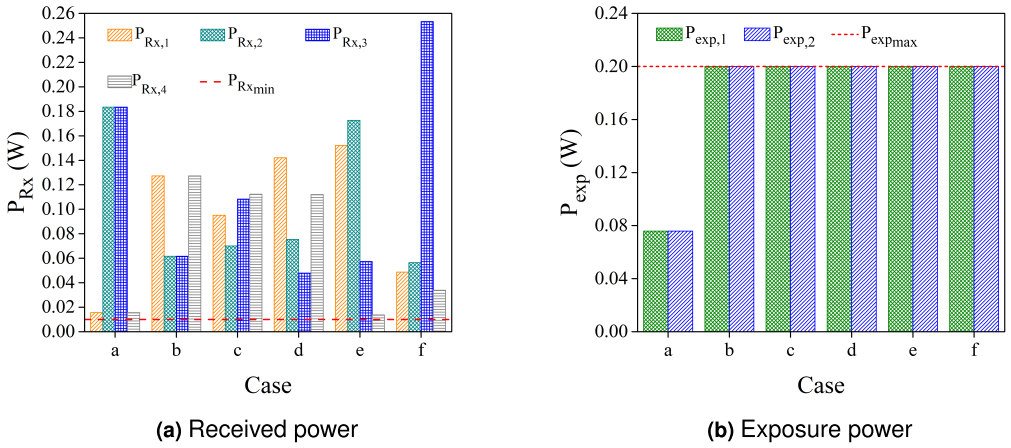

FIGURE 16. Received power and RF radiation exposure power of four receivers and two people case.

in Fig. 18(d) and (f), the power beacon reduces the energy toward the receiver, which is located near the human body. A slight intensity difference between the experiment and simulation is still found due to the reflection phenomenon that could happen in the indoor propagation environment not fully surrounded by the anechoic absorber. However, in

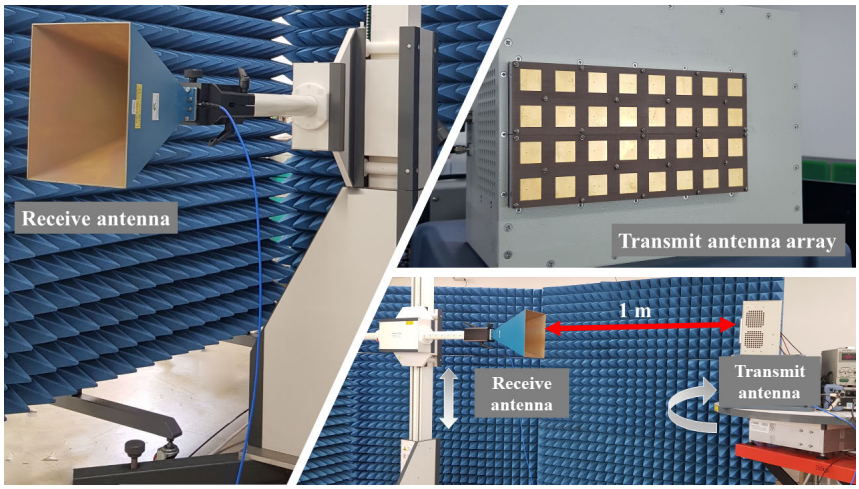

FIGURE 17. Experimental setup for beam shape measurement.

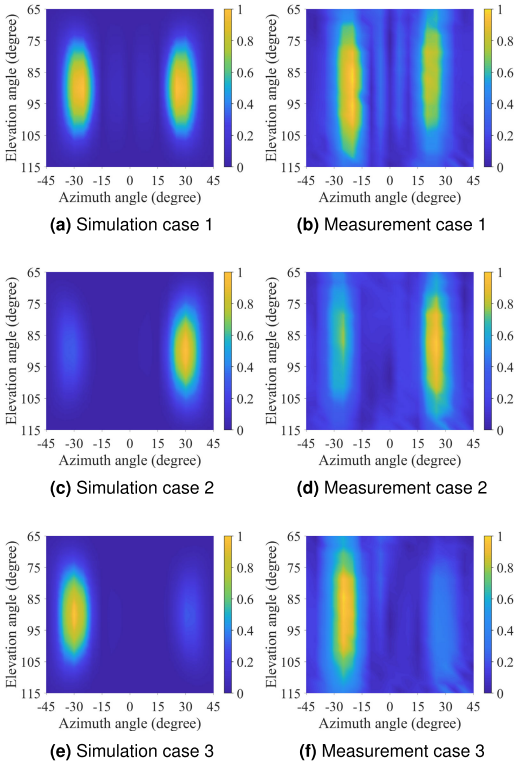

FIGURE 18. Comparison between the simulated and measured beam pattern in the normalized scale (i.e., case 1: human body at (3.5 m, 0 m), case 2: human body at (3.5 m, −1.5 m), and case 3: human body at (3.5 m, 1.5 m)).

general, the experimental results successfully verify that the proposed EVD/PSG algorithm can be applied in the real testbed environment.

VI. CONCLUSION

In this paper, we have presented two algorithms, the semidefinite relaxation (SDR) and the eigenvalue decomposition/projected subgradient (EVD/PSG) methods, to avoid the RF-EMF overexposure in the WPT environment. We have analyzed the system model, derived the algorithms, and proved that the simulation results agree with the analytical results. Based on the simulation results, we have confirmed that the RF-EMF exposure to the human body can be modeled using the far-field approach for defining the position of human body in the WPT area. We have also verified that through the iterative hierarchical scheme, in which the eigenvalue decomposition and projected subgradient dual method are applied, the EVD/PSG algorithm can obtain the near-optimal solution as the obtained results match the SDR results. By experiments, we have shown that the experimental results match the simulation result which implies the EVD/PSG algorithm can be applied in the real experimental environment. Therefore, we can conclude that both the proposed algorithms successfully maximize the received power while maintaining the RF-EMF exposure toward the human body below the safety restriction.

REFERENCES

[1] H.-D. Lang, A. Ludwig, and C. D. Sarris, "Maximum transfer efficiency and optimal loads for WPT systems with multiple transmitters," in *Proc. IEEE Antennas Propag. Soc. Int. Symp. (APSURSI)*, Memphis, TN, USA, Jul. 2014, pp. 430–431.

[2] S. Goguri, R. Mudumbai, and A. Kruger, "Optimizing wireless power transfer with multiple transmitters," in *Proc. 51st Annu. Conf. Inf. Sci. Syst. (CISS)*, Baltimore, MD, USA, Mar. 2017, pp. 1–5.

[3] L. Tan, S. Pan, X. Huang, and C. Xu, "System optimization for wireless power transfer system with double transmitters," in *Proc. IEEE PELS Workshop Emerg. Technol., Wireless Power Transf. (WoW)*, Chongqing, China, May 2017, pp. 1–3.

[4] Z. Wang, L. Duan, and R. Zhang, "Adaptively directional wireless power transfer for large-scale sensor networks," *IEEE J. Sel. Areas Commun.*, vol. 34, no. 5, pp. 1785–1800, May 2016.

[5] S. Kashyap, E. Bjornson, and E. G. Larsson, "Can wireless power transfer benefit from large transmitter arrays?" in *Proc. IEEE Wireless Power Transf. Conf. (WPTC)*, Boulder, CO, USA, May 2015, pp. 1–3.

[6] T. A. Khan, A. Yazdan, and R. W. Heath, Jr., "Optimization of power transfer efficiency and energy efficiency for wireless-powered systems with massive MIMO," *IEEE Trans. Wireless Commun.*, vol. 17, no. 11, pp. 7159–7172, Nov. 2018.

[7] A. Costa, R. Goncalves, P. Pinho, and N. B. Carvalho, "Beam steering antenna and network design for WPT applications," in *Proc. 10th Eur. Conf. Antennas Propag. (EuCAP)*, Davos, Switzerland, Apr. 2016, pp. 1–4.

[8] L. Yang, Y. Zeng, and R. Zhang, "Wireless power transfer with hybrid beamforming: How many RF chains do we need?" *IEEE Trans. Wireless Commun.*, vol. 17, no. 10, pp. 6972–6984, Oct. 2018.
[9] L. R. Varshney, "Transporting information and energy simultaneously," in *Proc. IEEE Int. Symp. Inf. Theory*, Toronto, ON, Canada, Jul. 2008, pp. 1612–1616.
[10] F. Zhu, F. Gao, Y. C. Eldar, and G. Qian, "Robust simultaneous wireless information and power transfer in beamspace massive MIMO," *IEEE Trans. Wireless Commun.*, vol. 18, no. 9, pp. 4199–4212, Sep. 2019.
[11] L. Liu, R. Zhang, and K.-C. Chua, "Multi-antenna wireless powered communication with energy beamforming," *IEEE Trans. Commun.*, vol. 62, no. 12, pp. 4349–4361, Dec. 2014.
[12] S. Bi, C. K. Ho, and R. Zhang, "Wireless powered communication: Opportunities and challenges," *IEEE Commun. Mag.*, vol. 53, no. 4, pp. 117–125, Apr. 2015.
[13] A. Ahmad, R. Ariffin, N. M. Noor, and M. Adzmey Sagiruddin, "1.8 GHz radio frequency signal radiation effects on human health," in *Proc. IEEE Int. Conf. Control Syst., Comput. Eng.*, Penang, Malaysia, Nov. 2011, pp. 546–550.
[14] K. A. Ansal, D. S. Jose, and R. K. Rajan, "Review on biological effect of electromagnetic radiation," in *Proc. Int. Conf. Circuits Syst. Digit. Enterprise Technol. (ICCSDET)*, Kottayam, India, Dec. 2018, pp. 1–5.
[15] I. Nasim and S. Kim, "Human exposure to RF fields in 5G downlink," 2017, *arXiv:1711.03683*. [Online]. Available: http://arxiv.org/abs/1711.03683
[16] H. Mazar, *Radio Spectrum Management: Policies, Regulations, and Techniques*. Hoboken, NJ, USA: Wiley, 2016.
[17] Z.-Q. Luo, W.-K. Ma, A. So, Y. Ye, and S. Zhang, "Semidefinite relaxation of quadratic optimization problems," *IEEE Signal Process. Mag.*, vol. 27, no. 3, pp. 20–34, May 2010.
[18] S. Boyd and L. Vandenberghe, *Convex Optimization*. New York, NY, USA: Cambridge Univ. Press, 2004.
[19] B. Ghojogh, F. Karray, and M. Crowley, "Eigenvalue and generalized eigenvalue problems: Tutorial," 2019, *arXiv:1903.11240*. [Online]. Available: http://arxiv.org/abs/1903.11240
[20] K. S. Yildirim, R. Carli, and L. Schenato, "Safe distributed control of wireless power transfer networks," *IEEE Internet Things J.*, vol. 6, no. 1, pp. 1267–1275, Feb. 2019.
[21] K. S. Yildirim, R. Carli, and L. Schenato, "Distributed control of wireless power transfer subject to safety constraints," in *Proc. IFAC*, Toulouse, France, Apr. 2017, pp. 13210–13215.
[22] R. Dai, Y. Zhao, G. Chen, W. Dou, C. Tian, X. Wu, and T. He, "Robustly safe charging for wireless power transfer," in *Proc. IEEE INFOCOM-IEEE Conf. Comput. Commun.*, Honolulu, HI, USA, Apr. 2018, pp. 378–386.
[23] H. Dai, Y. Liu, G. Chen, X. Wu, T. He, A. X. Liu, and H. Ma, "Safe charging for wireless power transfer," *IEEE/ACM Trans. Netw.*, vol. 25, no. 6, pp. 3531–3544, Dec. 2017.
[24] J. Zhang, G. Zheng, I. Krikidis, and R. Zhang, "Specific absorption rate-aware beamforming in MISO downlink SWIPT systems," *IEEE Trans. Commun.*, vol. 68, no. 2, pp. 1312–1326, Feb. 2020.
[25] K. Kurokawa, "Power waves and the scattering matrix," *IEEE Trans. Microw. Theory Techn.*, vol. 13, no. 2, pp. 194–202, Mar. 1965.
[26] V. Y. Pan and Z. Q. Chen, "The complexity of the matrix eigenproblem," in *Proc. 31st Annu. ACM Symp. Theory Comput. (STOC)*, Atlanta, GA, USA, May 1999, pp. 507–516.

LORENZ GINTING received the B.S. degree in telecommunication engineering from the Institut Teknologi Bandung, Indonesia, in 2014, and the M.S. degree from the Department of Computer Science and Engineering, Seoul National University of Science and Technology, South Korea, in 2017. She is currently pursuing the Ph.D. degree with the Department of Electrical and Computer Engineering, Sungkyunkwan University, South Korea. Her research interests include RF energy transfer and beamforming.

HYUN SIK YOON received the B.S. degree in electrical electronic engineering from Sungkyunkwan University, South Korea, in 2020, where he is currently pursuing the M.S. degree with the College of Information and Communication Engineering. His research interest includes 5G mobile communications.

DONG IN KIM (Fellow, IEEE) received the Ph.D. degree in electrical engineering from the University of Southern California, Los Angeles, CA, USA, in 1990. He was a tenured Professor with the School of Engineering Science, Simon Fraser University, Burnaby, BC, Canada. Since 2007, he has been an SKKU-Fellowship Professor with the College of Information and Communication Engineering, Sungkyunkwan University (SKKU), Suwon, South Korea. He is a Fellow of the Korean Academy of Science and Technology and a member of the National Academy of Engineering of Korea. He has been a first recipient of the NRF of Korea Engineering Research Center in Wireless Communications for RF Energy Harvesting since 2014. He was selected as the 2019 recipient of the IEEE Communications Society Joseph LoCicero Award for Exemplary Service to Publications. He is also the Executive Chair of IEEE ICC 2022 in Seoul. He has been listed as a 2020 Highly Cited Researcher by Clarivate Analytics. From 2001 to 2020, he served as an editor and an editor-at-large for Wireless Communication I for the IEEE TRANSACTION ON COMMUNICATIONS. From 2002 to 2011, he has served as an Editor and the Founding Area Editor of cross-layer design and optimization for the IEEE TRANSACTIONS ON WIRELESS COMMUNICATIONS. From 2008 to 2011, he has served as the Co-Editor-in-Chief for the IEEE/KICS JOURNAL OF COMMUNICATIONS AND NETWORKS. He has served as the Founding Editor-in-Chief for the IEEE WIRELESS COMMUNICATIONS LETTERS from 2012 to 2015.

KAE WON CHOI (Senior Member, IEEE) received the B.S. degree in civil, urban, and geosystem engineering and the M.S. and Ph.D. degrees in electrical engineering and computer science from Seoul National University, Seoul, South Korea, in 2001, 2003, and 2007, respectively. From 2008 to 2009, he was with Telecommunication Business of Samsung Electronics Company Ltd., South Korea. From 2009 to 2010, he was a Postdoctoral Researcher with the Department of Electrical and Computer Engineering, University of Manitoba, Winnipeg, MB, Canada. From 2010 to 2016, he was an Assistant Professor with the Department of Computer Science and Engineering, Seoul National University of Science and Technology, South Korea. In 2016, he joined the Faculty at Sungkyunkwan University, Korea, where he is currently an Associate Professor with the College of Information and Communication Engineering. His research interests include RF energy transfer, metasurface communication, visible light communication, cellular communication, cognitive radio, and radio resource management. He has been serving as an Editor for the IEEE COMMUNICATIONS SURVEYS AND TUTORIALS since 2014, and an Editor for the IEEE WIRELESS COMMUNICATIONS LETTERS since 2015, IEEE TRANSACTIONS ON WIRELESS COMMUNICATIONS since 2017, and IEEE TRANSACTIONS ON COGNITIVE COMMUNICATIONS AND NETWORKING since 2019.